https://doi.org/10.1016/j.apenergy.2020.115732

Energy-efficient decentralized control method with enhanced robustness for multi-evaporator air conditioning systems*

Zi-Yang Zhang[a,b], Chun-Lu Zhang[a,*], Fu Xiao[b]

[a]*Institute of Refrigeration and Cryogenics, School of Mechanical Engineering, Tongji University, Shanghai, China*

[b]*Research Institute for Sustainable Urban Development, The Hong Kong Polytechnic University, Hong Kong, China*

Abstract

Multi-evaporator air conditioning system has found increasing applications in buildings. Energy-efficient control for this kind of system presents significant challenge because of strong coupling effects and various operation modes. Existing control methods are most likely to encounter uncontrollable problems and lack robustness under uncertain operation conditions. This paper proposes an energy-efficient decentralized control method with enhanced robustness for multi-evaporator air conditioning system. The proposed method is featured by a self-optimizing control strategy and a decentralized proportional-integral (PI) control algorithm based on the effective open-loop transfer function (EOTF). Different from most of previous studies that regulated compressor speed to control the evaporating pressure by using a supervisory optimizer, the proposed self-optimizing control strategy regulates compressor speed to maintain constant suction superheat and achieves energy-efficient operation in a simple and robust manner. Meanwhile, the EOTF-based decentralized PI algorithm overcomes the weakness of decentralized controllers in dealing with coupling effects, while retaining robustness against model errors and component faults. Control performance of the proposed method is tested using a validated system dynamic model. Through extensive controllability tests, it is found that the proposed control method significantly improves temperature control performance of the conventional strategy. Up to 8.6% energy savings are achieved with the proposed control strategy. Moreover, the proposed EOTF-based PI controller demonstrates enhanced robustness in comparison with an advanced model predictive controller.

Keywords: air conditioning system; multi-evaporator; control; robustness; energy saving

---

* The short version of the paper was presented at ICAE2019, Aug 12-15, Västerås, Sweden. This paper is a substantial extension of the short version of the conference paper.

* Corresponding author. Tel.: +86-136-71825-133. *E-mail address*: chunlu.zhang@gmail.com (C.-L. Zhang)

Nomenclature

A	area (m^2)
A_r	area ratio between inside heat transfer area and outside heat transfer area
c_p	specific heat at constant pressure (kJ kg^{-1} K^{-1})
c_w	specific heat of tube wall (kJ kg^{-1} K^{-1})
D	diameter (m)
G(s)	transfer function
h	specific enthalpy (kJ kg^{-1})
L	tube length (m)
m	mass flow rate (kg s^{-1})
p	pressure (kPa)
Q	heat transfer capacity (W)
T	temperature (°C, K)
T_i	indoor air temperature (°C, K)
t	time (s)
V_i	volume of indoor space (m^3)

Greek symbol

α	heat transfer coefficient (W m^{-2} K^{-1})
ρ	density (kg m^{-3})
γ	void fraction

Subscripts

c	condensing
comp	compressor
DB	dry bulb
e	evaporating
e1, e2	two-phase and superheated region of the evaporator
ea	air flowing through the evaporator
ei, eo	evaporator inlet and outlet
eint	saturated gas cross-section of the evaporator
ew	tube wall of the evaporator
ge, le	saturated gas and saturated liquid at the evaporating pressure

ref	refrigerant
s	suction
sh	refrigerant superheat leaving the evaporator
ssh	refrigerant superheat at compressor suction port
WB	wet bulb

Abbreviations

COP	coefficient of performance
EOTF	effective open-loop transfer function
EXV	electronic expansion valve
IAE	integral absolute error
IMC	internal model control
MPC	model predictive control
PI	proportional-integral
S.P	setpoint
VRF	variable refrigerant flow

1 Introduction

Nowadays building air conditioning systems account for a large portion in building energy consumptions. For instance, 35% of total electricity consumptions of residential buildings in Hong Kong are attributed to air conditioning systems [1]. Among them, multi-evaporator air conditioning system, also called as variable refrigerant flow (VRF) system, is a popular configuration. It usually consists of one outdoor unit and multiple indoors units and is able to meet cooling demands of multiple zones simultaneously. Because of its independent and flexible zoning control mode, VRF system has been found to consume less energy than conventional variable air volume (VAV) system [2]. Besides, merits in design flexibility and installation convenience also contribute to the wide applications of VRF system. In China, VRF system takes 50.35% of the commercial air conditioning market in 2018 [3]. In view of the increasing applications of VRF system, its energy-efficient control is critical for reducing building energy consumptions. Yet it presents significant challenge to effectively control VRF system because of strong coupling effects between multiple indoor units and various operation modes when certain indoor units are switched-on or -off. Extensive research has therefore been conducted on the control of multi-evaporator air conditioning system.

Existing research on control of VRF system can be classified into two categories. The first category is centralized multi-input multi-output (MIMO) control, which considers multiple control loops as a whole, and generates control law based on a fairly accurate dynamic model of the VRF system. The most widely used MIMO control algorithms in literature are LQR (linear quadratic regulator) control [4, 5], model predictive control [6], and ANN (artificial neuron network) -based control [7]. Previous work [4, 6, 8] has shown that MIMO controllers are effective in reducing coupling effects and present satisfying control performance for multi-evaporator system. However, considering that VRF system usually operates in variable modes when different indoor units are switched on, developing a model-based MIMO controller for VRF system is not quite tractable [6, 9]. Furthermore, even in the same operation mode, there exists significant nonlinearity in fluid properties and components characteristics [10]. The strong nonlinearity is likely to result in model mismatch in the model-based controller and cause inferior control performance at operation points far away from the design point.

The second category is decentralized single-input single-output (SISO) control, which treats multiple control loops independently and can be achieved by using conventional

proportional-integral (PI) algorithm, without the need of accurate dynamic model. Because of its simplicity and robustness [11], decentralized control is more desirable for practical applications. This can be confirmed from dozens of manufacturers' patents [12-15]. While acknowledging the inherent limitations of decentralized control in handling loop couplings, it is practically significant to improve its control performance. For a multi-evaporator air conditioning system depicted in Fig.1, the manipulated variables (MV) include compressor speed and EXV (electronic expansion valve) openings. Indoor fan speed is normally regulated by users and is not an available manipulated variable. Decentralized control methods for the two MVs proposed in previous studies are summarized in Table 1. It can be found that the variable-speed compressor is usually controlled to satisfy the total cooling demand by either directly controlling cooling capacity [16], or inferentially controlling suction pressure p_s (or saturation suction temperature) [17-23]. Particularly, the variable target suction pressure scheme which determines suction pressure setpoint using optimization techniques shows encouraging energy performance [21, 23]. EXV openings are manipulated to simultaneously control indoor air temperature T_i and refrigerant superheat T_{sh} leaving the evaporators [16, 19, 24-26], so as to meet cooling demand of each indoor space, while preventing the compressor from liquid droplet. According to the reports from leading manufacturers [22], similar strategies in which compressor speed controls total cooling capacity and EXV controls both T_i and T_{sh} are widely adopted in commercialized VRF products. It will be termed as conventional strategy hereinafter.

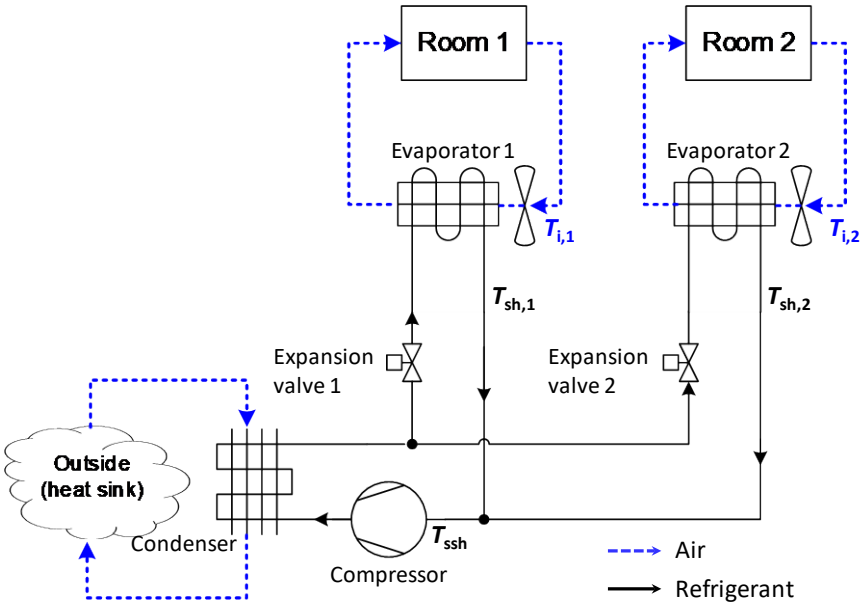

Fig.1 Schematic of a multi-evaporator air conditioning system

Table 1 Existing decentralized control methods for VRF system

MV	Reference	Year	Controlled variable	Remarks
Compressor speed	Chen et al. [18]	2005	Suction pressure p_s	Constant p_s target
	Lin and Yeh [19]	2009	Evaporating temperatures T_e	Preset T_e target
	Tu et al. [20]	2011	Average suction pressure p_s of digital scroll compressor	Constant p_s target
	Elliott et al. [27]	2013	Suction pressure p_s	MPC supervisor calculates p_s setpoint
	Xu et al. [16]	2013	Cooling capacity	Cooling capacity target is determined by operational indoor units
	Zhao et al. [21]	2015	Evaporating temperatures T_e	Variable T_e target
	Yun et al. [23]	2016	Evaporating temperatures T_e	T_e target is determined using load responsive method.
	Yan et al. [26]	2017	Refrigerant mass flow rate	High-low control strategy
	Tu et al. [28]	2018	Suction pressure p_s	p_s target is modified by gas pipe temperature.
EXV opening	Chen et al. [18]	2005	Indoor air temperature T_i	Fuzzy control
	Lin and Yeh [19]	2009	Indoor air temperature T_i and refrigerant superheat T_{sh}	Cascade control
	Shi et al. [24]	2013	Indoor air temperature T_i and refrigerant superheat T_{sh}	EXV controls T_i while ensuring smallest T_{sh}
	Xu et al. [16]	2013	Indoor air temperature T_i and refrigerant superheat T_{sh}	EXV controls T_{sh} when T_i was higher than its setpoint, and gets fully closed when the setpoint was met.
	Yan et al. [26]	2017	Indoor air temperature T_i and refrigerant superheat T_{sh}	Aims to improve humidity control performance
	Li et al. [25]	2017	Indoor air temperature T_i and refrigerant superheat T_{sh}	

Although the conventional control strategy is widely adopted, it implies two limitations that have not been closely examined in previous studies. Firstly, the conventional strategy manipulates compressor speed mainly based on the feedback signal of suction pressure. Variable target suction pressure scheme shows significant energy-saving potential [21, 23]. Nevertheless, determining an energy-efficient suction pressure setpoint which ensures the

compressor output capacity to precisely match the cooling load under variable operation conditions is a challenging task. The methods proposed by previous studies usually rely on an accurate performance prediction model [7, 23, 27]. Considering modeling error and operation uncertainties, it is difficult to always reach the optimal suction pressure setpoint under various conditions. Secondly, using only one input, i.e. the indoor EXV opening, to control two variables, i.e. T_{sh} and T_i , actually contradicts with functional controllability theory [11]. Functional controllability implies independent control of all outputs with available inputs. It requires that the number of inputs should at least equal to the number of outputs. Therefore, the conventional strategy is likely to cause uncontrollable problems in meeting control objectives of T_{sh} and T_i simultaneously.

To address the above-mentioned problems with the conventional strategy, this paper proposes a different control strategy for multi-evaporator air conditioning system, which regulates the compressor speed to maintain constant suction superheat T_{ssh}, and regulates the indoor EXV openings to maintain indoor air temperature T_i. The proposed control strategy avoids the EXV control being overridden by assigning only one controlled variable in its control loop. Moreover, different from the variable target suction pressure required by the conventional strategy, the proposed strategy maintains constant suction superheat to regulate compressor output capacity. It offers an alternative method to achieve energy-efficient operation with improved control strategy. This research attempts to verify the advantages of the proposed strategy in terms of temperature control performance and energy efficiency through extensive controllability tests. Decentralized proportional-integral (PI) controller is developed for the proposed strategy. To deal with coupling effects among multiple control loops, the effective open-loop transfer function (EOTF) [29] is for the first time introduced to the refrigeration control field to finely tune the decentralized controllers. In short, this paper makes new contributions in two aspects. First, the proposed control strategy avoids uncontrollable problems of conventional strategy and achieves energy-efficient operation in a simple manner. Second, the EOTF-based control algorithm overcomes the weakness of conventional decentralized controllers in dealing with coupling effects.

Fig.2 shows how the paper is organized. Section 2 introduces the proposed energy-efficient decentralized control method. Section 3 presents the dynamic modeling and validation of a two-evaporator air conditioning system to develop a virtual testbed for controllability tests. Section 4 details the design of a PI controller based on the proposed decentralized control method, and another two controllers for comparisons. Section 5

evaluates the performance of the proposed control method with regard to temperature control performance, energy efficiency and robustness through a comprehensive comparison study. Section 6 summarizes the conclusions and major contributions of this study.

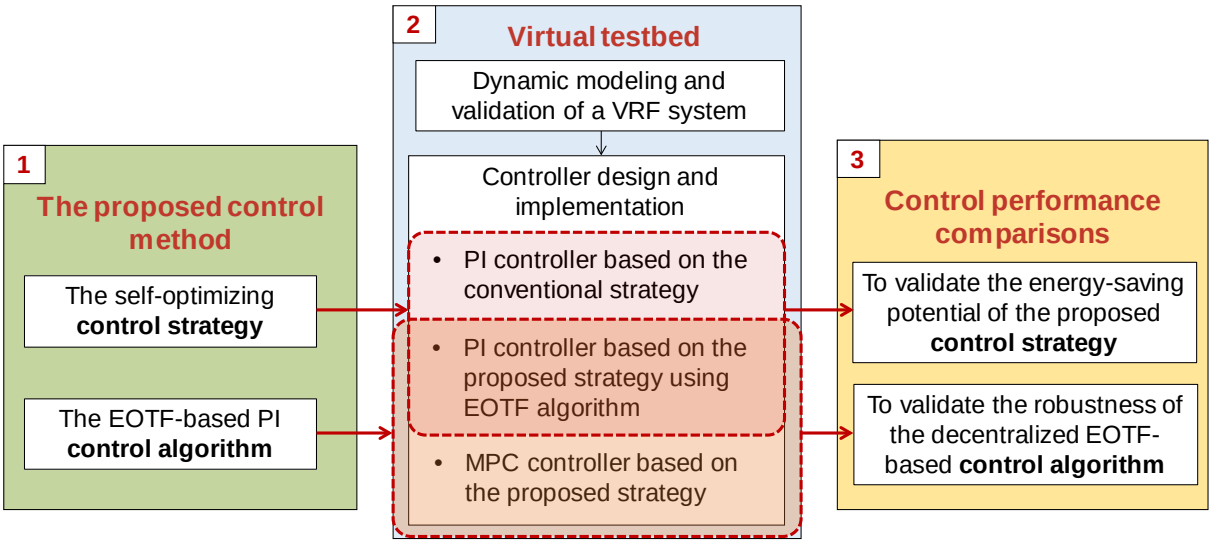

Fig.2 Flowchart of this paper

2 The proposed energy-efficient decentralized control method

The proposed decentralized control method for VRF system makes new contributions in two aspects: the energy-efficient control strategy and the EOTF-based PI control algorithm. This section details the development of the proposed control method and clarifies its novelty in the two aspects.

2.1 Energy-efficient control strategy based on self-optimizing approach

The proposed decentralized control strategy regulates the compressor speed to maintain constant suction superheat T_{ssh}, and regulates the indoor EXV openings to maintain indoor air temperature T_i in the corresponding rooms. Since the setpoints for controlled variables T_{ssh} and T_i hold constant or purely rely on user settings, it is actually a “self-optimizing” scheme. The notion “self-optimizing control” is proposed by Skogestad [30-32] in process control field. It refers to control strategy which achieves optimal operation with constant setpoint policy and avoids complicated real-time optimization of the setpoints of controlled variables [31]. The mechanism of the proposed control strategy in achieving energy-efficient optimal operation is explained with the illustrative example below.

Consider a case that the setpoint of the first indoor air temperature $T_{i,1}$ decreases and setpoints of the second indoor air temperature $T_{i,2}$ and suction superheat T_{ssh} remain unchanged (refers to Fig.1). According to the proposed control strategy, EXV openings of the first indoor unit (EXV1) increase so as to meet the increased cooling demand. As a result, less refrigerant flow is fed into the second indoor unit and the second indoor air temperature $T_{i,2}$ may slightly increase [33]. Larger openings of EXV2 are requisite in this case to deliver the required refrigerant to the second indoor unit. More refrigerant mass flow thereby enters the compressor and causes smaller suction superheat T_{ssh}. The compressor speed then increases to maintain constant T_{ssh}. In this way, the output capacity of the variable-speed compressor matches with the increased cooling load and the indoor air temperature settings are precisely satisfied. More notably, the optimal suction pressure p_s is automatically obtained by controlling a constant suction superheat T_{ssh}. The reason is that same cooling capacity of the VRF system can be achieved with different combinations of suction superheat and evaporating temperature [21]. By allocating a small target T_{ssh}, typically to be 5°C, the proposed control strategy can always reach the maximal available suction pressure that ensures sufficient cooling capacity under various operation conditions. Therefore, the optimal operation of the VRF system in terms of energy efficiency is achieved.

Different from previous study that relies on supervisory controller to achieve optimal operation [7, 23, 27], the proposed control strategy seeks optimal suction pressure merely with a constant T_{ssh} and is therefore simpler and more robust. On the other aspect, the proposed strategy assigns only one controlled variable T_i in EXV control loop and allocates the remaining controlled variable, refrigerant superheat T_{sh} to the compressor which controls the mixed overall suction superheat T_{ssh}. It thereby effectively solves the functional uncontrollable problem of the conventional strategy.

Although the control strategy proposed here is simple, easy-to-implement, reliable and energy-efficient, it ignores the coupling effects between multiple control loops. Therefore, new control algorithms which can effectively alleviate the coupling effects, are needed.

2.2 EOTF-based PI control algorithm considering coupling effects

The proportional-integral (PI) control algorithm is a dominant control algorithm in HVAC systems [34, 35]. PI controllers usually work in each control loop separately and there is little collaboration among individual PI controller and control loop. Therefore, this kind of controller is essentially incompetent to deal with coupling effects of different control loops. In this study, an improved PI control algorithm based on EOTF (effective open-loop transfer

function) is developed for the VRF system. EOTF of loop i is defined as the transfer function relating input u_i with output y_i when only loop i is open and all other loops are closed [29]. The effect of the other loops on a particular control loop is effectively expressed with EOTF. Once EOTF is obtained, any PI tuning method can be applied to design individual PI controller based on the corresponding EOTF. The resulting PI controller takes dynamic interactions into account. Previous research from control field has established that decentralized PI controllers designed based on EOTF provide satisfactory performance with weak interactions, fast responses, and good robustness [29, 36, 37].

According to the proposed control strategy, the two-evaporator air conditioning system depicted in Fig.1 can be regarded as a three-input three-output system. The three inputs are compressor speed and openings of EXV1 and EXV2. The three outputs are suction superheat T_{ssh} and indoor air temperature $T_{i,1}$ and $T_{i,2}$. The open-loop transfer function can be written as

$$\mathbf{G}(s)=\begin{bmatrix} g_{11}(s) & g_{12}(s) & g_{13}(s) \\ g_{21}(s) & g_{22}(s) & g_{23}(s) \\ g_{31}(s) & g_{32}(s) & g_{33}(s) \end{bmatrix} \tag{1}$$

To obtain EOTF of the 1st control loop $G_{eff,1}$, a matrix equation based on the open loop transfer function $\mathbf{G}(s)$ is formulated as $\mathbf{G}(s)\mathbf{U} = \mathbf{Y}$, where $\mathbf{Y}$ is [1 0 0] and represents the open-loop control of the 1st output, and closed-loop control of the 2nd and 3rd output. The solution $\mathbf{U}$ to the above equation indicates the required input vector to achieve the control objectives dictated by output vector $\mathbf{Y}$. EOTF of the 1st control loop $G_{eff,1}$ is then attained by taking the inverse of the first element u_1 in $\mathbf{U}$. EOTFs for the other two control loops can be deduced with the same approach.

For the two-evaporator air conditioning system depicted in Fig.1, the analytical solutions of EOTFs are constituted as Eq. (2), where det $\mathbf{G}$ represents the determinant of transfer function matrix $\mathbf{G}$(s).

$$\begin{cases} G_{\text{eff},1}=\dfrac{\det\ \mathbf{G}}{g_{22}g_{33}-g_{32}g_{23}} \\ G_{\text{eff},2}=\dfrac{\det\ \mathbf{G}}{g_{11}g_{33}-g_{13}g_{31}} \\ G_{\text{eff},3}=\dfrac{\det\ \mathbf{G}}{g_{11}g_{22}-g_{12}g_{21}} \end{cases} \tag{2}$$

When the number of indoor units and EXV increases, EOTFs for such systems with higher dimensions can be obtained using the method introduced in Xiong et al. [36] and Shen

et al. [38], of which the computation load will not significantly increase owing to the inverse matrix approximation techniques.

3 Dynamic modeling of a two-evaporator air conditioning system

In this section, a physics-based dynamic model for a two-evaporator VRF system integrated with room thermal model is developed so as to establish a virtual testbed for the proposed control method. The dynamic model is validated using experiment data.

3.1 Model development

3.1.1 Heat exchangers

Dynamic models of evaporators and condenser are developed based on the moving-boundary method [39, 40]. The following details the dynamic modeling of the evaporator.

The evaporator can be divided into a two-phase region and a superheated region as shown in Fig.2. The governing equations include mass and (or) energy equations of refrigerant, tube wall and air in both two-phase and superheated regions. Assumptions taken in the model are the same as [39].

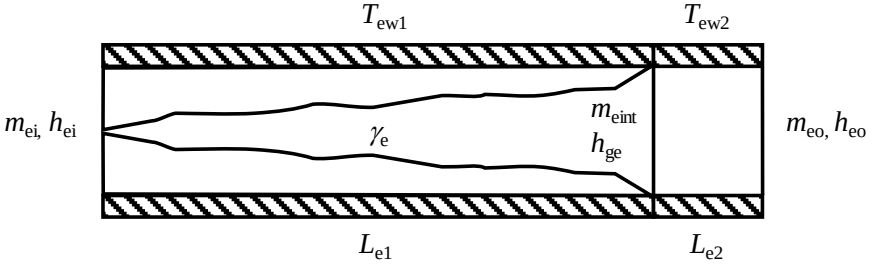

Fig.3 Schematic of the evaporator model

Refrigerant mass and energy conservation equations of two-phase region can be expressed as below. Note that the superscript dot in the below equations represents derivative of the corresponding parameter with respect to time.

$$\left(\rho_{le}-\rho_{ge}\right)\left(1-\overline{\gamma}_e\right)A_e\dot{L}_{e1}+\left(\frac{\mathrm{d}\rho_{le}}{\mathrm{d}p_e}\left(1-\overline{\gamma}_e\right)+\frac{\mathrm{d}\rho_{ge}}{\mathrm{d}p_e}\overline{\gamma}_e\right)A_eL_{e1}\dot{p}_e=m_{ei}-m_{eint} \tag{3}$$

$$\begin{aligned}&\left(\rho_{\mathrm{le}}h_{\mathrm{le}}-\rho_{\mathrm{ge}}h_{\mathrm{ge}}\right)\left(1-\overline{\gamma}_{\mathrm{e}}\right)A_{\mathrm{e}}\dot{L}_{\mathrm{e1}}+\left(\frac{\mathrm{d}\rho_{\mathrm{le}}h_{\mathrm{le}}}{\mathrm{d}p_{\mathrm{e}}}\left(1-\overline{\gamma}_{\mathrm{e}}\right)+\frac{\mathrm{d}\rho_{\mathrm{ge}}h_{\mathrm{ge}}}{\mathrm{d}p_{\mathrm{e}}}\overline{\gamma}_{\mathrm{e}}-1\right)A_{\mathrm{e}}L_{\mathrm{e1}}\dot{p}_{\mathrm{e}}\\&=m_{\mathrm{ei}}h_{\mathrm{ei}}-m_{\mathrm{eint}}h_{\mathrm{ge}}+\alpha_{\mathrm{e1,\,ref}}\pi D_{\mathrm{e}}L_{\mathrm{e1}}\left(T_{\mathrm{ew1}}-T_{\mathrm{e}}\right)\end{aligned}\tag{4}$$

Refrigerant energy conservation equation of superheated region is

$$\begin{aligned}&\rho_{\mathrm{ge}}\frac{h_{\mathrm{ge}}-h_{\mathrm{s}}}{2}A_{\mathrm{e}}\dot{L}_{\mathrm{e1}}+\left(\frac{\rho_{\mathrm{ge}}}{2}\left(\frac{\mathrm{d}h_{\mathrm{ge}}}{\mathrm{d}p_{\mathrm{e}}}+\frac{\partial h_{\mathrm{s}}}{\partial p_{\mathrm{e}}}\right)-1\right)A_{\mathrm{e}}L_{\mathrm{e2}}\dot{p}_{\mathrm{e}}+\frac{\rho_{\mathrm{ge}}}{2}\frac{\partial h_{\mathrm{s}}}{\partial T_{\mathrm{s}}}A_{\mathrm{e}}L_{\mathrm{e2}}\dot{T}_{\mathrm{s}}\\&=m_{\mathrm{eint}}\left(h_{\mathrm{ge}}-h_{\mathrm{s}}\right)+\alpha_{\mathrm{e2,\,ref}}\pi D_{\mathrm{e}}L_{\mathrm{e2}}\left(T_{\mathrm{ew2}}-\left(T_{\mathrm{e}}+T_{\mathrm{s}}\right)/2\right)\end{aligned}\tag{5}$$

Energy equation for the tube wall of two-phase region is based on the weighted mean wall temperature [41].

$$\begin{aligned}&\rho_{\mathrm{w}}c_{\mathrm{w}}A_{\mathrm{w}}\frac{L_{\mathrm{e1}}}{L_{\mathrm{e}}}\left(T_{\mathrm{ew1}}-T_{\mathrm{ew2}}\right)\dot{L}_{\mathrm{e1}}+\rho_{\mathrm{w}}c_{\mathrm{w}}A_{\mathrm{w}}L_{\mathrm{e1}}\dot{T}_{\mathrm{ew1}}\\&=\alpha_{\mathrm{e1,\,ref}}\pi D_{\mathrm{e}}L_{\mathrm{e1}}\left(T_{\mathrm{e}}-T_{\mathrm{ew1}}\right)+\alpha_{\mathrm{e,\,air}}\pi D_{\mathrm{e}}L_{\mathrm{e1}}\left(T_{\mathrm{ea1}}-T_{\mathrm{ew1}}\right)/A_{\mathrm{r}}\end{aligned}\tag{6}$$

Energy equation for the tube wall of superheated region is

$$\begin{aligned}&\rho_{\mathrm{w}}c_{\mathrm{w}}A_{\mathrm{w}}\frac{L_{\mathrm{e2}}}{L_{\mathrm{e}}}\left(T_{\mathrm{ew1}}-T_{\mathrm{ew2}}\right)\dot{L}_{\mathrm{e1}}+\rho_{\mathrm{w}}c_{\mathrm{w}}A_{\mathrm{w}}L_{\mathrm{e2}}\dot{T}_{\mathrm{ew2}}\\&=\alpha_{\mathrm{e2,ref}}\pi D_{\mathrm{e}}L_{\mathrm{e2}}\left[\left(T_{\mathrm{e}}+T_{\mathrm{s}}\right)/2-T_{\mathrm{ew2}}\right]+\alpha_{\mathrm{e,air}}\pi D_{\mathrm{e}}L_{\mathrm{e2}}\left(T_{\mathrm{ea2}}-T_{\mathrm{ew2}}\right)/A_{\mathrm{r}}\end{aligned}\tag{7}$$

For the air side, dynamics of air flow is ignored. Energy equation of air flow in the two-phase region is

$$m_{\mathrm{ea}}c_{\mathrm{p,a}}\mathrm{d}T_{\mathrm{ea}}=\alpha_{\mathrm{e,air}}\pi D_{\mathrm{e}}\mathrm{d}L_{\mathrm{e}}\left(T_{\mathrm{ew1}}-T_{\mathrm{ea}}\right)/A_{\mathrm{r}}\tag{8}$$

By integrating Eq. (8) over two-phase region, air temperature at refrigerant saturation vapor point is

$$T_{\mathrm{ea,x1}}=\left(T_{\mathrm{ea,in}}-T_{\mathrm{ew1}}\right)\exp\left(-\frac{\alpha_{\mathrm{e,air}}\pi D_{\mathrm{e}}}{m_{\mathrm{ea}}c_{\mathrm{p,a}}A_{\mathrm{r}}}L_{\mathrm{e1}}\right)+T_{\mathrm{ew1}}\tag{9}$$

With the same approach, air temperature leaving the evaporator is given by

$$T_{\mathrm{ea,out}}=\left(T_{\mathrm{ea,x1}}-T_{\mathrm{ew2}}\right)\exp\left(-\frac{\alpha_{\mathrm{e,air}}\pi D_{\mathrm{e}}}{m_{\mathrm{ea}}c_{\mathrm{p,a}}A_{\mathrm{r}}}L_{\mathrm{e2}}\right)+T_{\mathrm{ew2}}\tag{10}$$

Equations (3) through (7) describe the major dynamics of an evaporator. Equations (9)

and (10) are used to calculate air temperature leaving the evaporator and heat transfer capacity. The compact matrix-equation form of the evaporator can be written as

$$\mathbf{F}_e \dot{\mathbf{X}}_e = G(\mathbf{X}_e, \mathbf{U}_e) \tag{11}$$

where $\mathbf{X}_e = [p_e, L_{e1}, T_s, T_{ew1}, T_{ew2}]$, is the vector of five state variables in the evaporator model.

Dynamic modeling of the condenser applies the same approach as the evaporator, except that the condenser is divided into desuperheating region, two-phase region and subcooling region. Due to limited space, details of governing equations shall not be described here.

3.1.2 Compressor

The dynamics of refrigerant mass flow rate through the compressor is much faster than that of the heat exchangers [42]. Therefore, a steady-state polynomial equation [43] is selected to predict the variable-speed compressor performance, as shown in Eq. (12).

$$\begin{aligned} y_{comp} = {} & c_1 + c_2 T_e + c_3 T_c + c_4 f_r + c_5 T_e^2 + c_6 T_c^2 + c_7 f_r^2 + c_8 T_e T_c + c_9 T_e f_r + c_{10} T_c f_r \\ & + c_{11} T_e^2 f_r + c_{12} T_e f_r^2 + c_{13} T_c^2 f_r + c_{14} T_c f_r^2 + c_{15} T_e T_c f_r \end{aligned} \tag{12}$$

where y denotes refrigerant mass flow rate or power consumption of compressor, and T_c, T_e, f_r stand for the condensing temperature, evaporating temperature, and compressor frequency, respectively. Coefficients c_1 to c_{15} are curve-fitted using the data provided by compressor manufacturer.

3.1.3 Expansion valve

Since the dynamic response of expansion valve is also faster than that of the heat exchangers, steady state equation is used for calculating refrigerant mass flow rate through the EXV, as given by Eq. (13). In Eq. (13), the discharge coefficient C_{exv} is determined empirically or from manufacturer information [42]. EXV opening area A_{exv} can be expressed as a function of EXV opening pulses. ρ, p_i and p_o represent refrigerant density at the inlet port and refrigerant pressure at the inlet and outlet port of the EXV, respectively.

$$m_{exv} = C_{exv} A_{exv} \sqrt{\rho (p_i - p_o)} \tag{13}$$

3.1.4 Indoor spaces

The dynamics of indoor air temperature T_i can be described by the following equation.

$$\rho_{\mathrm{a}} c_{\mathrm{p,a}} V_{\mathrm{i}} \frac{dT_{\mathrm{i}}}{dt} = m_{\mathrm{ea}} c_{\mathrm{p,a}} \left(T_{\mathrm{ea,out}} - T_{\mathrm{i}}\right) + Q_{\mathrm{inter}} + U_{\mathrm{i}} A_{\mathrm{i}} \left(T_{\mathrm{o}} - T_{\mathrm{i}}\right) \tag{14}$$

where indoor air temperature T_{i} equals to air temperature entering the evaporator $T_{\mathrm{ea,in}}$ in Eq. (9). The first term in the right side of Eq. (14) represents cooling capacity provided by the evaporator, the second and third term represent space cooling load resulted from internal heat gains and external heat gains, respectively.

3.1.5 System modeling

A main challenge in modeling refrigeration system with multiple evaporators is the mass flow distribution among evaporators. Dynamically, refrigerant mass flow rate entering the evaporator equals to that passing through the upstream EXV. Refrigerant mass flow rate leaving the evaporator is calculated by Eq. (15).

$$\begin{cases} m_{\mathrm{eo},1} = \sqrt{\dfrac{p_{\mathrm{e1}} - p_{\mathrm{e}}}{K}} \\ m_{\mathrm{eo},2} = \sqrt{\dfrac{p_{\mathrm{e2}} - p_{\mathrm{e}}}{K}} \\ m_{\mathrm{eo},1} + m_{\mathrm{eo},2} = m_{\mathrm{comp}} \end{cases} \tag{15}$$

where K is the pressure drop coefficient in the evaporator. p_{e}, p_{e1}, and p_{e2} represent compressor suction pressure and evaporating pressure of the two evaporators, respectively.

Dynamic model of the VRF system is developed by integrating the component models together, as per

$$\mathbf{F}\,\dot{\mathbf{X}} = G\left(\mathbf{X}, \mathbf{U}\right) \tag{16}$$

To facilitate further controller design and controllability tests, the nonlinear dynamic model Eq. (16) is linearized into a state-space form. Deviation variables $\delta\mathbf{X}$ and $\delta\mathbf{U}$ in the vicinity of an equilibrium point are introduced to approximately describe system dynamics, as given by Eq. (17).

$$\begin{cases} \mathbf{X} = \mathbf{X}^{\mathrm{s}} + \delta\mathbf{X}, \\ \mathbf{U} = \mathbf{U}^{\mathrm{s}} + \delta\mathbf{U}, \\ \delta G = \left.\dfrac{\partial G}{\partial \mathbf{X}}\right|_{\mathbf{X}^{\mathrm{s}}} \delta\mathbf{X} + \left.\dfrac{\partial G}{\partial \mathbf{U}}\right|_{\mathbf{U}^{\mathrm{s}}} \delta\mathbf{U} \end{cases} \tag{17}$$

The linear dynamic model is then developed as

$$\begin{cases} \dot{\mathbf{X}} = \mathbf{AX} + \mathbf{BU}, \mathbf{A} = \mathbf{F}^{-1}\dfrac{\partial G}{\partial \mathbf{X}},\ \mathbf{B} = \mathbf{F}^{-1}\dfrac{\partial G}{\partial \mathbf{U}} \\ \mathbf{Y} = \mathbf{CX} + \mathbf{DU} \end{cases} \tag{18}$$

where **X**, **U** and **Y** represent state variables, input variables and output variables, respectively.

3.2 Model validation

To validate the dynamic model developed in section 3.1, a test rig with a multi-evaporator air conditioning system is set up. The experimental VRF system consists of one condenser and four identical evaporators, with a rated cooling capacity of 12.8 kW. The VRF system supplies air at 19.6°C, which mainly handles sensible load and is known as high-temperature VRF system. System specifications are summarized in Table 2.

Table 2 Specifications of the experimental VRF system

Name	Specifications
Refrigerant	R410A
Compressor	Two identical rotary variable-speed compressors. Inner volume of the compressor cylinder is 17.2 cc.
EXV	Inside diameter 1.4 mm (for each)
Fan	Indoor fan: Four variable-speed centrifugal fans. Air flow rate for each fan is 1300 m^3/h when the fan runs at 435 rpm. Outdoor fan: Three variable-speed axial fans. Air flow rate for each fan is 2300 m^3/h when the fan runs at 550 rpm.
Condenser	9 circuits, 2 rows, 72 tubes per row, tube length: 1100 mm
Evaporator	3 circuits, 2 rows, 24 tubes per row, tube length: 750 mm (for each) Rated cooling capacity for each evaporator is 3.2 kW.

Notes: All heat exchangers are finned-tube coils with the same tube diameter 7.3 mm, tube pitch 22 mm, row pitch 19.05 mm, and two wave fins.

The VRF system was tested in a psychrometric room comprising one indoor chamber and one outdoor chamber, as shown in Fig.3 (a) and Fig.3 (b). Testing conditions for both environmental chambers are controlled by built-in air conditioning systems to be T_{DB} = 27°C and T_{WB} = 19°C, referring to Chinese standard [44]. A schematic of the experimental setup and major sensors is depicted in Fig.3 (c). Key operation parameters, including refrigerant temperatures and pressures at the compressor suction and discharge ports, refrigerant

temperature and pressure leaving each evaporator, and air temperature leaving each evaporator, are measured to record the dynamic response. The measurement instruments and their corresponding uncertainties are summarized in Table 3.

(a) Indoor chamber (b) Outdoor chamber

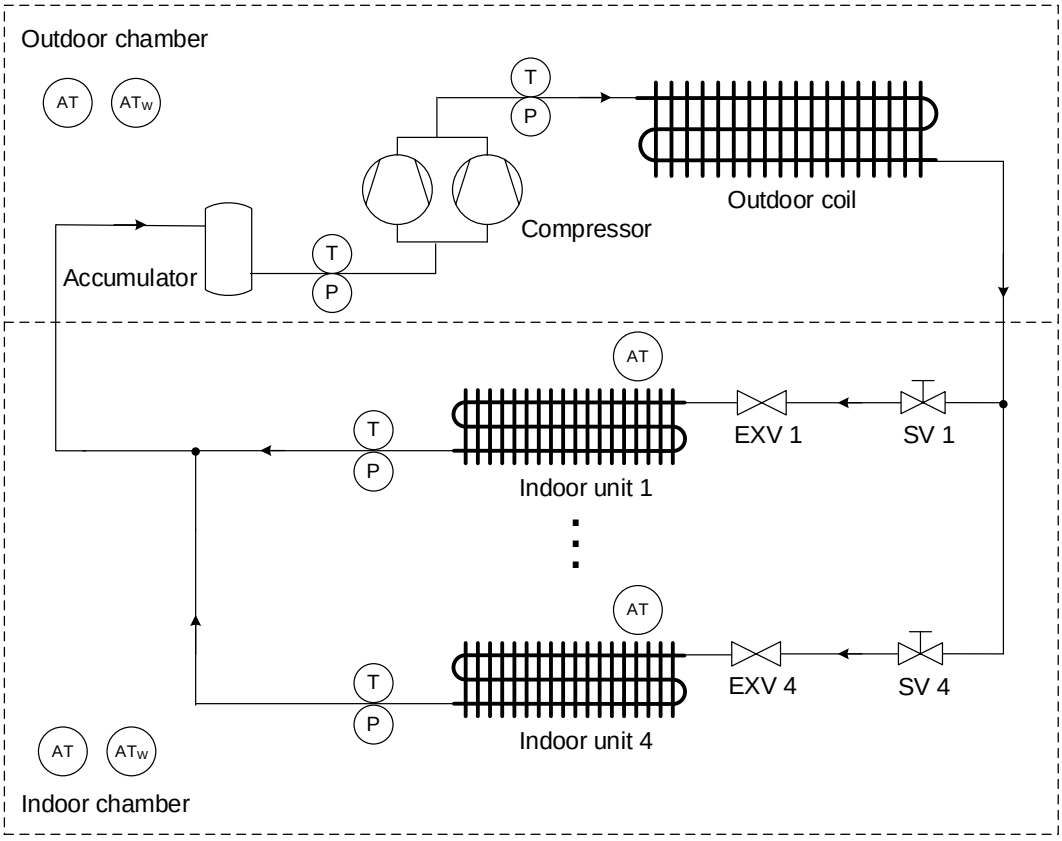

T – refrigerant temperature; P – refrigerant pressure; AT – air dry bulb; AT_W – air wet bulb

(c) Schematic of experimental setup

Fig.4 Experimental setup

Table 3 Summary of measuring instruments

Instrument	Sensor	Range	Accuracy
Thermal resistance	PT100 Class AA	-20–70 ºC	± 0.1 °C
Thermal couple	T type	-20–70 ºC	± 0.5 °C
Pressure transmitter	AP401	0–5000 kPa	± 0.25 % F.S.*

* F.S. stands for full scale.

In the experiments, two of the four indoor units are switched on to keep accordance with the dynamic model. Solenoid valves at the inlet of the switched-off indoor units are closed to avoid unwanted refrigerant migration. Outdoor and indoor fans run at 550 rpm and 435 rpm, respectively. Only one of the two compressors operates. Compressor speed and EXV openings are regulated manually to stimulate system dynamics, as shown in Fig.4. Close attention is paid during the experiments to assure that no refrigerant liquid droplet enters the compressor. Measuring signals of operation parameters are sent to personal computer for recording, with a sample time of 3 seconds.

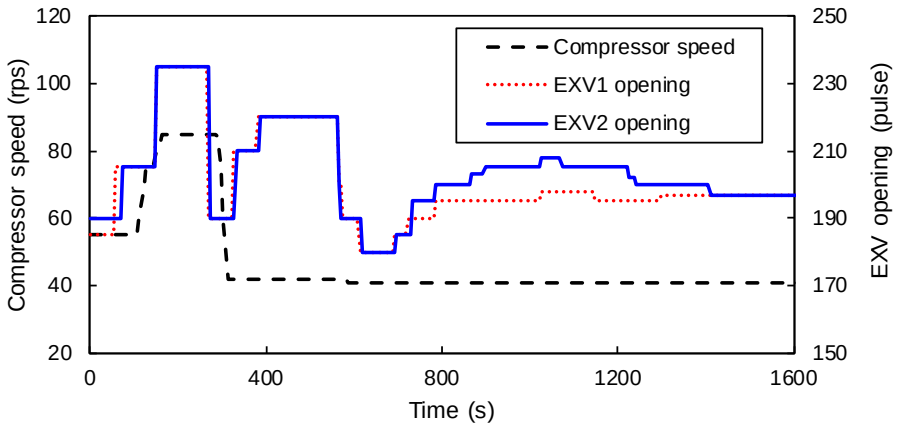

Fig.5 Testing signals for model validation

The same compressor speed and EXV openings as shown in Fig.4 are adopted as inputs of the dynamic model in validation test. Since evaporator inlet air temperature is fixed and no air circulation exists in experiments, the dynamic model is modified by removing governing equations of indoor thermal model. The simulated dynamic response of key operation parameters is compared with experimental results as shown in Fig.5. As observed, simulations based on the linear state-space model track the actual dynamic response reasonably well. Therefore, control performance analysis hereinafter will be conducted with the validated

dynamic model.

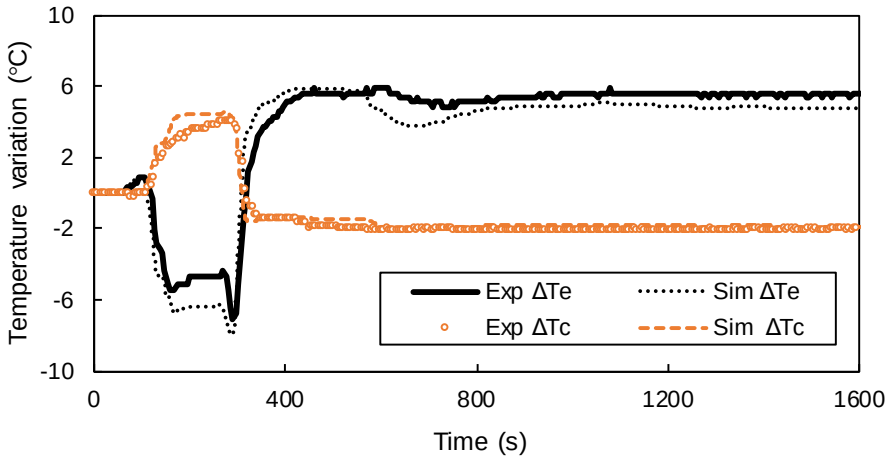

(a) Evaporating temperature and condensing temperature

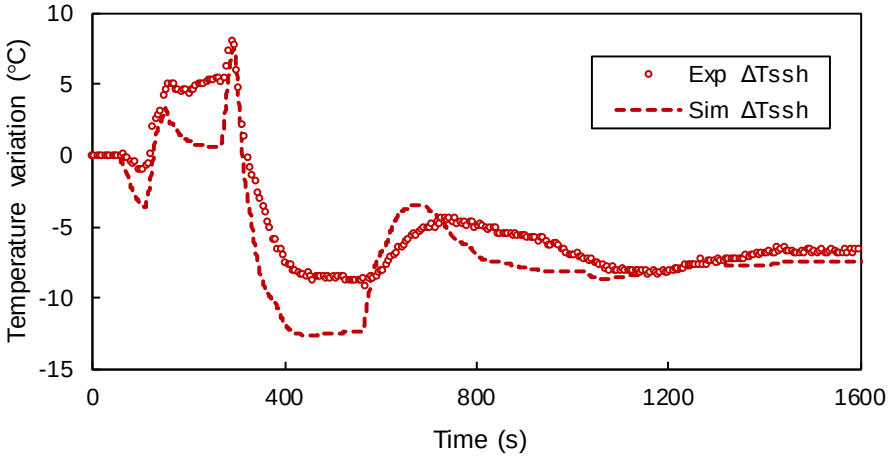

(b) Suction superheat

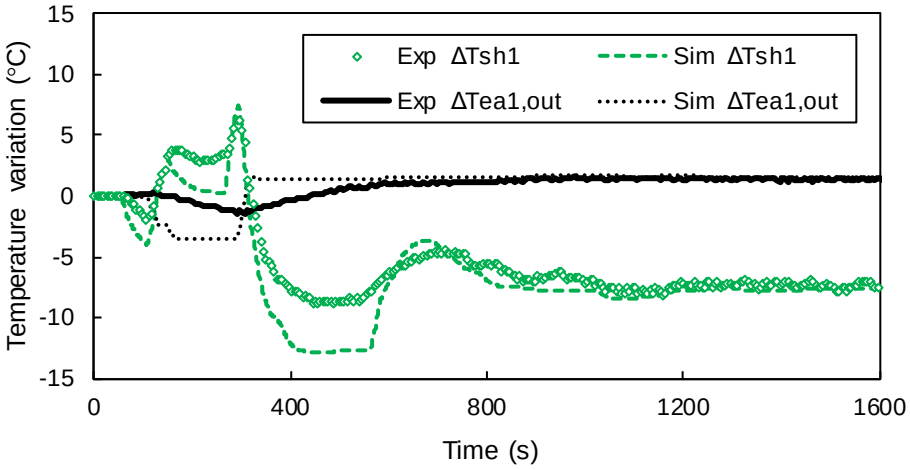

(c) Air leaving temperature and refrigerant superheat of evaporator 1

Fig.6 Comparisons of experimental and simulated outputs (Exp – experimental; Sim – simulated)

For the indoor thermal model that was not involved in validation test, the below model parameters are carefully determined. The area and height of each indoor space are assumed to be 16 m^2 and 3 m, respectively. UA value in Eq. (14) for calculating heat transfer rate between indoor air and outside is assumed to be 300 W/K. The ratio of cooling load resulted from internal heat gains to that resulted from external heat gains is approximately 1:3.

4 Controller design and implementation

In this section, the proposed decentralized control method is implemented and tested in the VRF system serving two rooms built on the testbed. A three-loop PI controller adopting the proposed EOTF-based PI control algorithm is developed. To map out improvements from the proposed control method, two other controllers are designed for comparison, in which the conventional PI controller is for the illustration of control performance resulted from different control strategies, while the model predictive controller using the same inputs and outputs as the proposed controller is for robustness comparison concerned with control algorithms. Control block diagrams of the three controllers are shown in Fig.6.

Notice that in the conventional strategy as illustrated by Fig.6(b), the compressor speed inferentially controls cooling capacity by constantly maintaining the sum of temperature control error to be zero, and EXV controls T_i with a deadband of ± 0.5°C referring to Xu et al. [16].

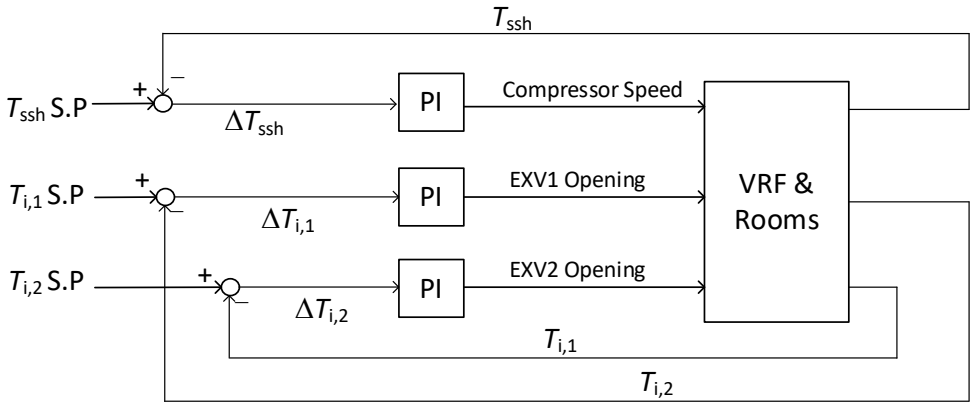

(a) Decentralized PI controller based on the proposed control strategy

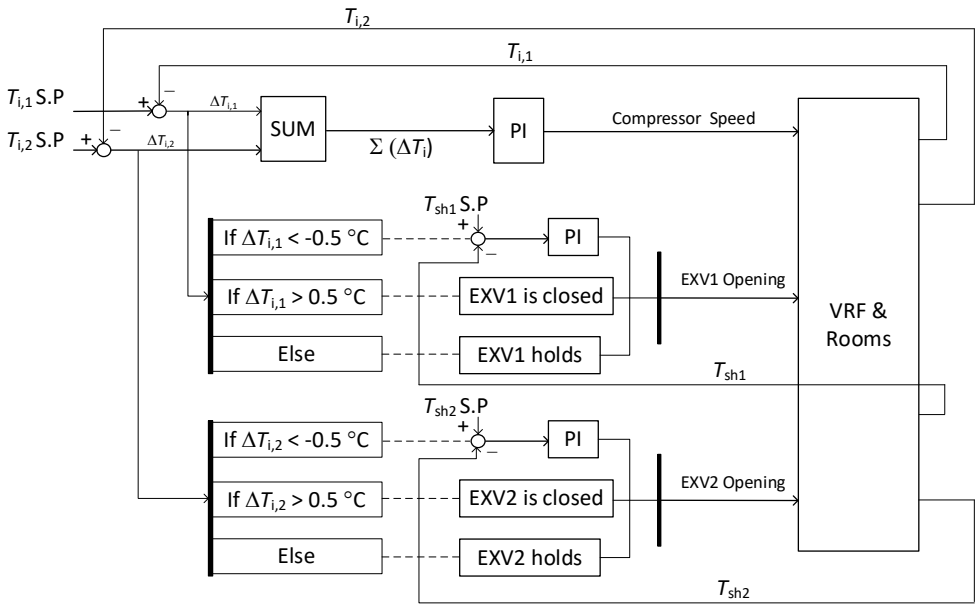

(b) Decentralized PI controller based on the conventional control strategy

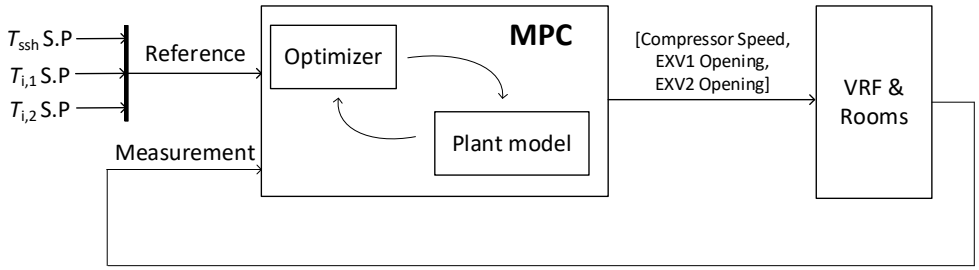

(c) Centralized model predictive controller adopting same inputs and outputs as the proposed control strategy

Fig.7 Control block diagrams

4.1 PI controller

The design of decentralized PI controllers employs IMC (internal model control)-PID method, referring to Lee et al. [45]. In the IMC-PID formulation, a controller based on the minimum phase part of the process transfer function is firstly deduced, with only one tuning parameter, namely the desired closed-loop time constant τ. The controller is then approximated into a PID controller by truncating high order terms using model reduction techniques. The IMC-PID method has gained widespread acceptance since it directly relates controller tuning with desired closed-loop performance and shows robustness to disturbances [45]. In this study, the improved PI controller is designed based on the effective open-loop transfer function (EOTF) of each control loop using IMC-PID method. When tuning PI

controllers, the selection of closed-loop time constant τ makes a trade-off between performance and robustness. The resulting controller parameters including proportional coefficient k_p and integral coefficient k_i, together with tuning parameter τ for the two decentralized controllers are summarized in Table 4.

Table 4 Decentralized controller parameters for VRF system

Control strategy	Control loop	τ (s)	k_p	k_i
Proposed strategy	Compressor - T_{ssh}	0.62	5.9	1.2
	EXV1 – $T_{i,1}$	120	-26	-0.13
	EXV2 – $T_{i,2}$	120	-26	-0.13
Conventional strategy	Compressor - ΣT_i	120	-2.3	-0.015
	EXV1 – $T_{sh,1}$	20	-2.0	-0.44
	EXV2 – $T_{sh,2}$	20	-2.0	-0.44

4.2 MPC controller

The mechanism of model predictive control (MPC) is to use a system model to predict the future evolution of a dynamic system over the prediction horizon N_p. It solves an optimization problem formulated as Eq. (19) to minimize predicted reference following error e and change of inputs Δu over the prediction horizon N_p. At each time step, the optimizer gives the optimal trajectory of control signals with N_c free variables (N_c is termed as control horizon). Only the first control signal is applied, whereas the rest of the control sequence is discarded. Then the prediction horizon shifts forward and repeats the same optimization process based on the updated measurements [46].

$$J = \sum_{i=1}^{N_p} W_e e_{k+i}{}^2 + \sum_{i=0}^{N_p-1} W_{\Delta u} \Delta u_{k+i}{}^2 \tag{19}$$

In this study, the internal predictive model used in the MPC controller is the linearized system dynamic model at rated cooling conditions where the compressor speed is 40 rps. A sample time of 1s is chosen to react to fast dynamics at refrigerant side. The prediction horizon and control horizon are 300 s and 30s, respectively, balancing control performance with computational complexity. The weighting matrix W_e and $W_{\Delta u}$ in Eq. (19) are determined by trial and error to reach comparable control performance with the decentralized PI controller. Note that the comparable control performance at design point is required since the centralized

MPC controller is designed to compare the robustness of the two control algorithms against model errors and component faults. The control parameters used in the centralized MPC controller are summarized in Table 5.

Table 5 MPC parameters

T_s (s)	N_p	N_c	W_e	$W_{\Delta u}$
1	300	30	$\begin{bmatrix} 3 \\ 0.6 \\ 0.6 \end{bmatrix}$	$\begin{bmatrix} 1 \\ 1 \\ 1 \end{bmatrix}$

Eventually, a virtual testbed is developed in MATLAB / Simulink environment by implementing the controllers in the validated system dynamic model. Controllability tests are conducted using this testbed.

5 Control performance analysis

In this section, temperature control performance, energy efficiency and robustness of the proposed decentralized controller are evaluated by comparing with the performance of the other two controllers.

5.1 Temperature control performance

A command following test where the setpoint of $T_{i,1}$ increases by 2°C at Time = 0 s, and setpoints of other controlled variables remain unchanged is performed. The simulation results are presented in Fig.7. Note that variables shown in vertical axis represent variations from the original conditions.

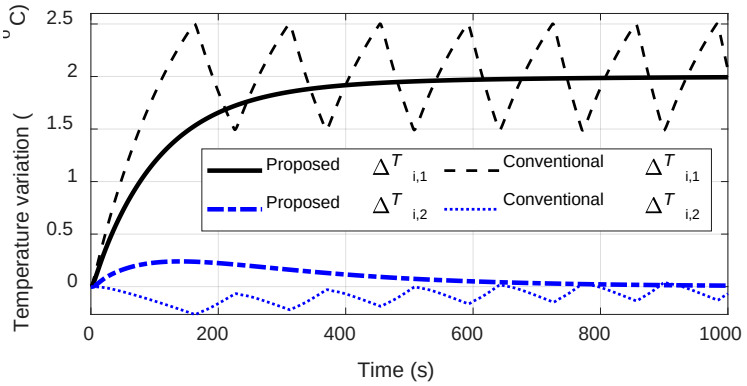

(a) Indoor air temperature

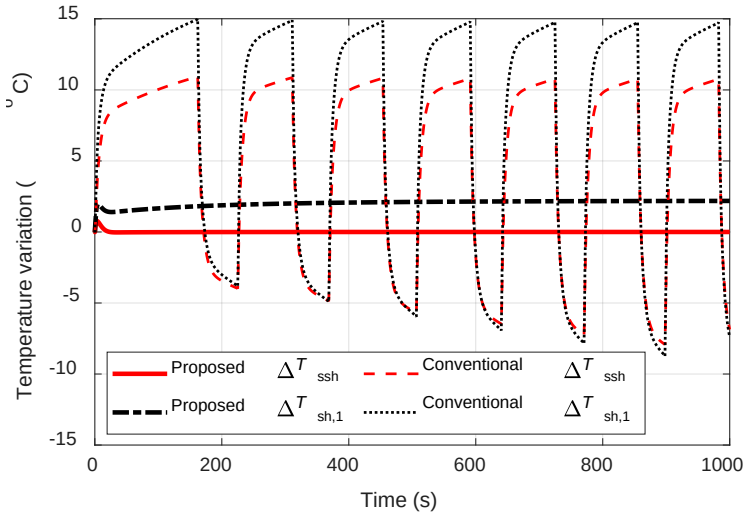

(b) Refrigerant superheat at compressor suction port and evaporator outlet

Fig.8 Dynamic response of controlled variables using proposed and conventional decentralized control strategy tracking increased room air temperature setpoint

As can be seen from Fig.7, there exist severe fluctuations in the dynamic response of T_i and T_{sh} using conventional control strategy. The fluctuation in indoor air temperature actually conforms with the experimental results reported in Xu et al. [16]. The reason is that conventional strategy attempts to simultaneously control T_i and T_{sh} with EXV openings. It requires that indoor air temperatures are maintained through switching-on and-off of indoor EXV and causes the control of T_{sh} based on PI algorithm to be frequently overridden. As a result, neither superheat T_{ssh} and T_{sh} nor indoor air temperature T_i gets stabilized. By comparison, controlled variables reach their setpoints smoothly and stably using the proposed control strategy as shown by solid lines in Fig.7. The proposed control strategy significantly improves temperature control performance of the VRF system.

The other set of controllability test examined the disturbance rejection performance of the two strategies, as shown in Fig.8, where the cooling load of 1st indoor space increases by 30% at Time = 0 s, and setpoints of controlled variables all remain unchanged. As expected, indoor air temperature $T_{i,1}$ increases at the beginning associated with the increased cooling load, which is similar for both controllers. But eventually, the proposed controller maintains indoor air temperature and suction superheat exactly with zero control error, while the conventional strategy provides fluctuated $T_{i,1}$ and T_{ssh}. The ability of the proposed control strategy in improving temperature control performance is further confirmed.

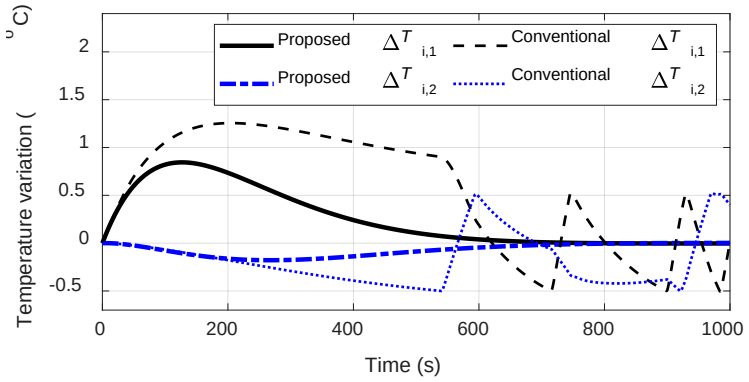

(a) Indoor air temperature

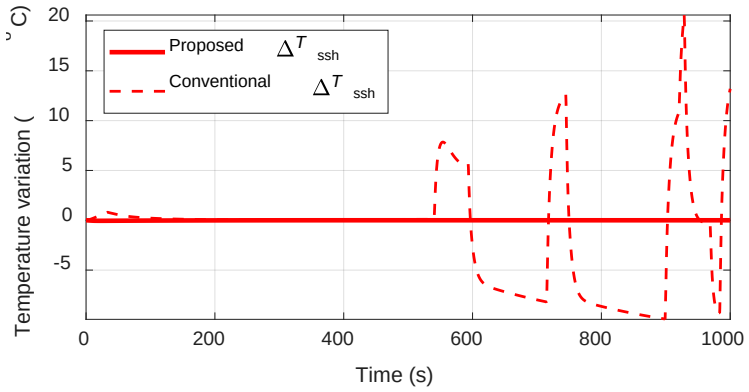

(b) Refrigerant superheat at compressor suction port

Fig.9 Dynamic response of controlled variables using proposed and conventional decentralized control strategy rejecting disturbances of increased space cooling load

5.2 Energy efficiency

Apart from improved temperature control performance, simulation results show that in the aforementioned two controllability tests, COP increases by 8.6% and 3.3%, respectively, compared with the conventional strategy. Here note that COP is defined over the duration when controlled variables stabilize within a predefined threshold. It can therefore be concluded that the proposed control strategy contributes to higher energy efficiency. The reason for relatively low COP using conventional strategy can be found from the dynamic response of manipulated variables in controllability tests shown in Fig.9. As seen, indoor EXV frequently switches -on and -off to maintain indoor air temperature, which leads to discontinuous cooling supply. Thus higher compressor speed is required for the conventional strategy when delivering same cooling capacity, as demonstrated in Fig.9(b). In contrast, the proposed strategy avoids cooling loss caused by on-off control of EXV and therefore consumes less compressor power consumptions. The results indicate that the proposed control

strategy achieves energy-efficient operation with appropriate choices of inputs and outputs, as well as reasonable inputs-outputs pairing decisions.

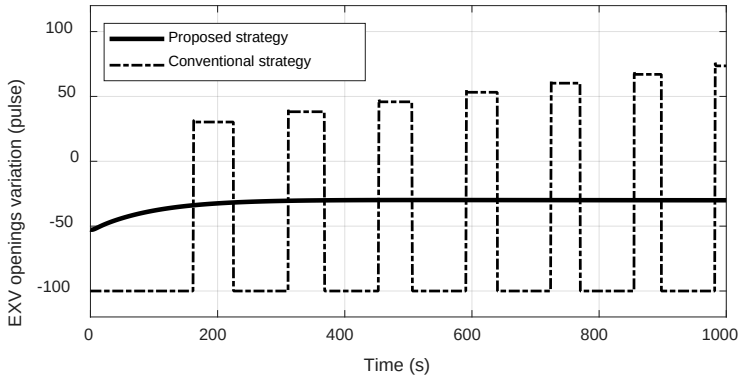

(a) EXV openings (Note that EXV opening of minus 100 pulses is used to simulate its closed status with the linearized dynamic model.)

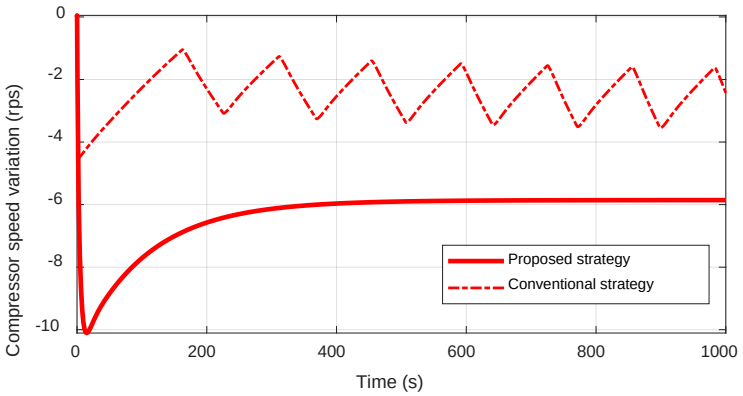

(b) Compressor speed

Fig.10 Dynamic response of manipulated variables using proposed and conventional decentralized control strategy tracking increased room air temperature setpoint

It might be concerned that the proposed strategy for VRF system will lead to poor energy performance when cooling demands of the two indoor units show large difference. In such a case, refrigerant leaving one evaporator is of two-phase state, while leaving the other with high superheat if we maintain a constant suction superheat. It implies relatively low heat transfer efficiency in the evaporators. However, such differentiated refrigerant outlet states are virtually unavoidable when handling uneven mass flow distribution with limited manipulated variables, i.e., compressor speed and EXV openings. Indoor air temperature T_{i} and refrigerant superheat heat T_{sh} leaving each evaporator are possible to be precisely controlled only in the ideal case that indoor fan speed is adjustable.

5.3 Robustness

To design a robust controller for multi-evaporator air conditioning system is one of the motivations of this research. This section aims to demonstrate the robustness of the proposed EOTF-based decentralized PI controller over the centralized MPC controller.

5.3.1 Control performance under off-design conditions

Control performance of decentralized PI controller and centralized MPC controller running over a wide range of conditions is to be evaluated for robustness comparisons. Command following tests are firstly performed under design conditions as baseline. Fig.10 compares the dynamic responses of controlled variables using the two controllers when setpoint of $T_{i,1}$ increases by 2°C. As seen, at design conditions, PI and MPC controllers yield similar performance in controlling $T_{i,1}$, whereas the MPC controller affords faster responses and smaller deviations in controlling T_{ssh} and $T_{i,2}$ than the PI controller. It is no surprise that MPC presents better performance since its control action relies on the knowledge about overall system dynamic characteristics. However, whether such merits of MPC controller preserve under off-design conditions is questionable.

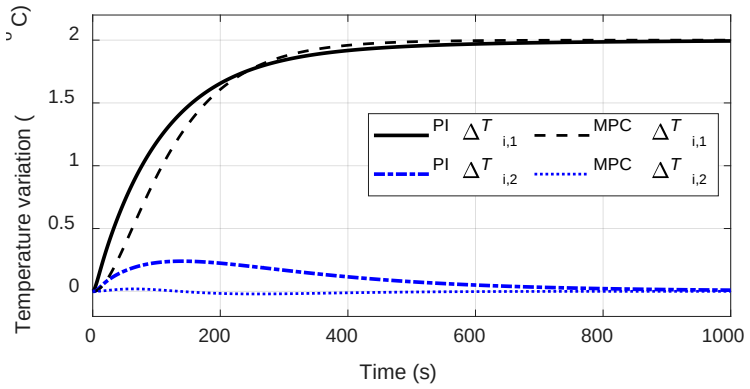

(a) Indoor air temperature

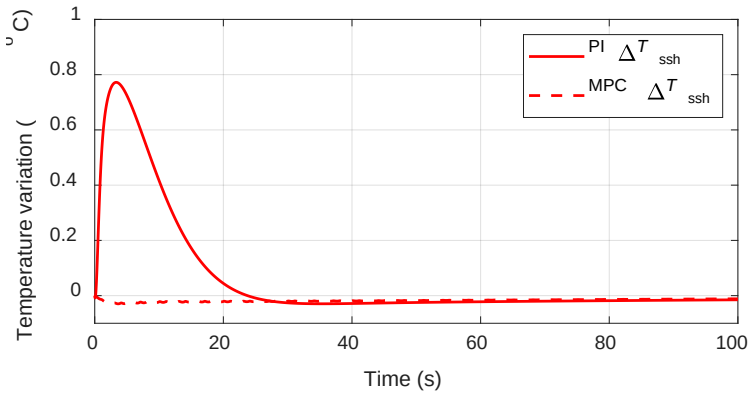

(b) Refrigerant superheat at compressor suction port

Fig.11 Control performance of EOTF-based decentralized PI controller and centralized MPC controller under design conditions

Dynamic models linearized at different steady equilibrium points by changing compressor speed are obtained to represent the real plant under off-design conditions. The same PI and MPC controllers as that were designed in section 4 are implemented in the new plant models. Here remind that the controllers are designed based on the dynamic model linearized when the compressor speed is 40 rps. Same command following tests as described in Fig.10 are performed with the newly obtained models. Two performance indexes are employed to quantify the control performance, namely settling time and integral absolute error (IAE). Settling time refers to the time it takes for the control error of $T_{i,1}$ to fall into 2% of its setpoint change. IAE is defined based on the control error of all the three controlled variables, as given by Eq. (20).

$$\mathrm{IAE} = \int_0^{\infty} \left(\left| e_{T_{ssh}} \right| + \left| e_{T_{i,1}} \right| + \left| e_{T_{i,2}} \right| \right) \mathrm{d}t \tag{20}$$

Comparisons between decentralized PI controller and centralized MPC controller in terms of the two performance indexes are summarized in Fig.11. What stands out in Fig.11 is that MPC yields a clear trend in increasing settling time and IAE when operation conditions get far away from the design conditions. The degradation of MPC performance is actually owing to the nonlinearity of refrigeration system, which causes model mismatch between the internal predictive model used in MPC and real plant model. In contrast, the two performance indexes using decentralized PI controller keep quite stable. Therefore, the robustness of the proposed EOTF-based PI controller is readily apparent.

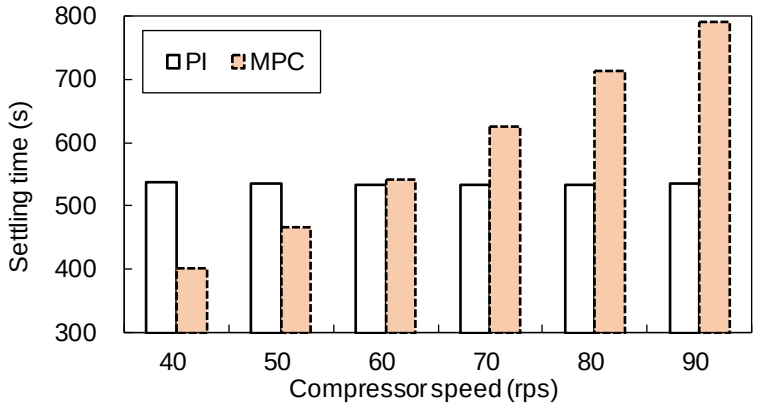

(a) Settling time

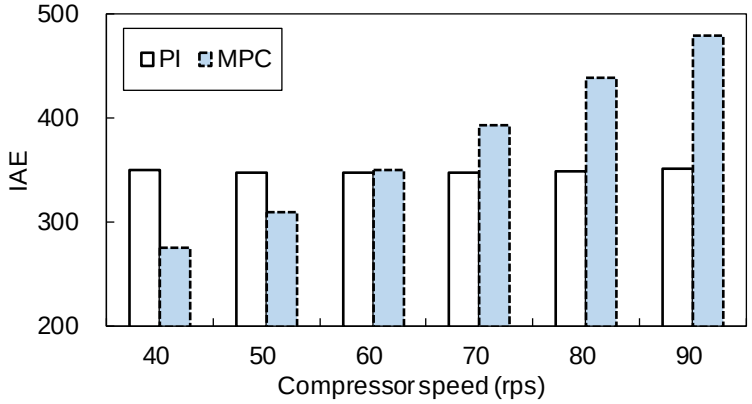

(a) Integral absolute error IAE

Fig.12 Comparisons of settling time and integral absolute error between EOTF-based decentralized PI controller and centralized MPC controller under off-design conditions

5.3.2 Control performance under component faults

As EXV actuators are frequent moving devices, they easily suffer from faults. This section compares the performance of the two algorithms when the EXV1 openings are unchangeable. Command following tests in which the setpoints of $T_{i,1}$ and $T_{i,2}$ decrease by 2°C and setpoint of T_{ssh} remains unchanged are performed using the two controllers. Results shown in Fig.12 indicate that $T_{i,1}$ with both controllers fails to satisfy its setpoint as expected since the most relevant actuator EXV1 is uncontrollable. As for the other two controlled variables $T_{i,2}$ and T_{ssh}, PI controller precisely maintains them to setpoints, while MPC results in steady-state deviations instead. It can be concluded that PI controller affords better robustness under component faults.

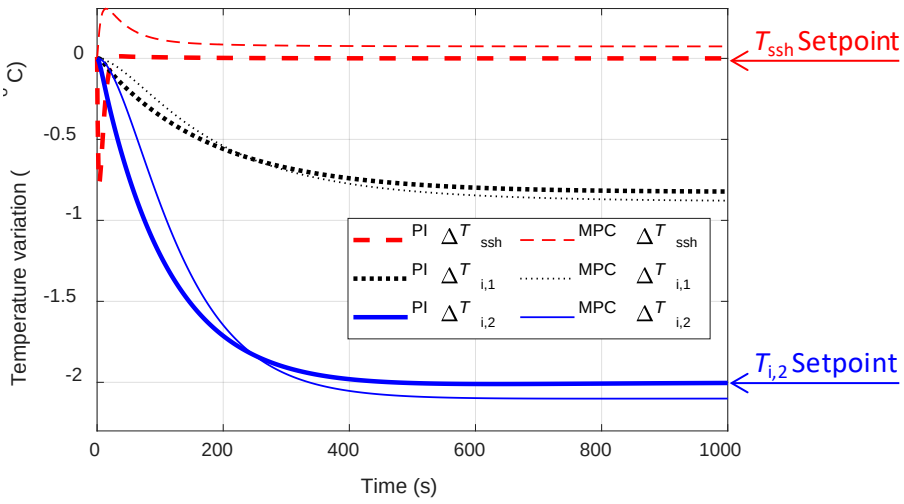

Fig.13 Control performance of EOTF-based decentralized PI controller and centralized MPC controller under component faults

The reason for the differentiated performance of decentralized PI controller and centralized MPC controller can be explained as below. Control behavior of centralized MPC controller comes down to finding the solution **U** to linear equations formulated as **GU** = **Y**, where **G** denotes 3-input 3-output system model, **U** and **Y** represent inputs and outputs. With given outputs target dictated by vector **Y**, there is unique solution **U** with a nonsingular **G**. Provided that one of the inputs is unable to follow solution **U** because of component faults, the output vector **Y** including three controlled variables will fail to satisfy the setpoints. By way of contrast, control behavior of decentralized PI controller is to find solutions of three independent equations. Component fault in one control loop does not affect the other two loops. As a consequence, the proposed decentralized control method for VRF system presents enhanced robustness thanks to its decentralized structure.

6 Conclusions

In this study, an energy-efficient decentralized control method with enhanced robustness for multi-evaporator air conditioning system is proposed. It makes contributions in two aspects: the self-optimizing control strategy, and the effective open-loop transfer function (EOTF)-based PI control algorithm. The self-optimizing control strategy suggests to regulate the compressor speed to maintain constant suction superheat, and regulate the indoor expansion valve openings to maintain indoor air temperature. The proposed control strategy achieves energy-efficient operation with constant setpoint, which is simple and robust for

industrial applications. The EOTF-based PI control algorithm tunes control parameters considering interactions among multiple control loops, and effectively handles coupling effects in the control of multi-evaporator air conditioning system.

Control performance of the proposed method is tested using a validated system dynamic model. Through a comprehensively comparative study, it is found that the proposed method improves temperature control performance and provides energy savings compared with the conventional strategy. Simulation results show that energy efficiency increases by 8.6% and 3.3% in a command following and disturbance rejection test, respectively. Furthermore, enhanced robustness for the proposed decentralized control method is verified in comparisons with a centralized model predictive controller.

Acknowledgements

This work is funded by the National Natural Science Foundation of China (Grant No. 51676140). The authors also gratefully acknowledge the financial support of Research Institute for Sustainable Urban Development (RISUD) of the Hong Kong Polytechnic University.

References

[1] Electrical and mechanical services department of Hong Kong Government, Hong Kong Energy End-use Data; 2018. https://wwwemsdgovhk/filemanager/en/content_762/HKEEUD2018pdf.

[2] Yu X, Yan D, Sun K, Hong T, Zhu D. Comparative study of the cooling energy performance of variable refrigerant flow systems and variable air volume systems in office buildings. Applied Energy. 2016;183:725-36.

[3] The commercial air conditioning market report of China in 2018. (in Chinese)

[4] Shah R, Alleyne AG, Bullard CW. Dynamic Modeling and Control of Multi-Evaporator Air-Conditioning Systems. ASHRAE Transactions. 2004;110:109-19.

[5] Yang Y, Wu M-D, Chang Y-C. Temperature control of the four-zone split inverter air conditioners using LMI expression based on LQR for mixed H2/H∞. Applied Energy. 2014;113:912-23.

[6] Koeln JP, Alleyne AG. Decentralized controller analysis and design for multi-evaporator vapor compression systems. Proceedings of the American Control Conference. Washington2013. p. 437-42.

[7] Kang I, Lee K, Lee J, Moon J. Artificial Neural Network–Based Control of a Variable Refrigerant Flow System in the Cooling Season. Energies. 2018;11:1643.

[8] Lee IH, Choi JW, Kim MS. Studies on the heating capacity control of a multi-type heat pump system applying a multi-input multi-output (MIMO) method. International Journal of Refrigeration. 2011;34:416-28.

[9] Lin X, Lee H, Hwang Y, Radermacher R. A review of recent development in variable refrigerant flow systems. Science and Technology for the Built Environment. 2015;21:917-33.

[10] He XD, Asada HH. A new feedback linearization approach to advanced control of Multi-Unit HVAC

Systems. Proceedings of the American Control Conference. Denver2003. p. 2311-6.
[11] Skogestad S, Postlethwaite I. Multivariable feedback control : analysis and design. Chichester, England: John Wiley; 2005.
[12] CN105571067A. Multiple online control method and system. 2016.
[13] CN103486692A. Load self-adaptation variable-frequency multi-connection heat pump system and method for controlling compressor frequency. 2014.
[14] CN106196495A. Control device and method for multi-split air conditioner and multi-split air conditioner 2016.
[15] CN106052216A. Method for controlling electronic expansion valves during multi-connected air conditioning unit heating. 2016.
[16] Xu X, Pan Y, Deng S, Xia L, Chan M. Experimental study of a novel capacity control algorithm for a multi-evaporator air conditioning system. Applied Thermal Engineering. 2013;50:975-84.
[17] Zhang G, Xiao H, Zhang P, Wang B, Li X, Shi W, et al. Review on recent developments of variable refrigerant flow systems since 2015. Energy and Buildings. 2019;198:444-66.
[18] Chen W, Zhou X, Deng S. Development of control method and dynamic model for multi-evaporator air conditioners (MEAC). Energy Conversion and Management. 2005;46:451-65.
[19] Lin J-L, Yeh TJ. Control of multi-evaporator air-conditioning systems for flow distribution. Energy Conversion and Management. 2009;50:1529-41.
[20] Tu Q, Dong K, Zou D, Lin Y. Experimental study on multi-split air conditioner with digital scroll compressor. Applied Thermal Engineering. 2011;31:2449-57.
[21] Zhao D, Zhang X, Zhong M. Variable evaporating temperature control strategy for VRV system under part load conditions in cooling mode. Energy and Buildings. 2015;91:180-6.
[22] Daikin. Maintenance handbook for VRV series: RUXYQ8-66AB. Shanghai: Daikin Air Conditioning Cooperation; 2014.
[23] Yun GY, Lee JH, Kim HJ. Development and application of the load responsive control of the evaporating temperature in a VRF system for cooling energy savings. Energy and Buildings. 2016;116:638-45.
[24] Shi W, Wang B, Shao S. Design of small capacity air conditioners and heat pumps (in Chinese). Beijing: China Architecture & Building Press; 2013.
[25] Li Z, Wang B, Li X, Shi W, Zhang S, Liu Y. Simulation of recombined household multi-split variable refrigerant flow system with split-type air conditioners. Applied Thermal Engineering. 2017;117:343-54.
[26] Yan H, Xia Y, Deng S. Simulation study on a three-evaporator air conditioning system for simultaneous indoor air temperature and humidity control. Applied Energy. 2017;207:294-304.
[27] Elliott MS, Rasmussen BP. Decentralized model predictive control of a multi-evaporator air conditioning system. Control Engineering Practice. 2013;21:1665-77.
[28] Tu Q, Zhang L, Cai W, Guo X, Yuan X, Deng C, et al. Control strategy of compressor and sub-cooler in variable refrigerant flow air conditioning system for high EER and comfortable indoor environment. Applied Thermal Engineering. 2018;141:215-25.
[29] Vu TNL, Lee M. Independent design of multi-loop PI/PID controllers for interacting multivariable processes. Journal of Process Control. 2010;20:922-33.
[30] Skogestad S. Self-optimizing control: the missing link between steady-state optimization and control. Computers & Chemical Engineering. 2000;24:569-75.
[31] Jensen JB, Skogestad S. Optimal operation of simple refrigeration cycles: PART II. Computers & Chemical Engineering. 2007;31:1590-601.
[32] Skogestad S. Near-optimal operation by self-optimizing control: from process control to marathon running

and business systems. Computers & Chemical Engineering. 2004;29:127-37.
[33] Matsumoto K, Ohno K, Yamaguchi S, Saito K. Numerical analysis of control characteristics of variable refrigerant flow heat-pump systems focusing on the effect of expansion valve and indoor fan. International Journal of Refrigeration. 2019;99:440-52.
[34] Chen Y, Yan H, Luo Y, Yang H. A proportional–integral (PI) law based variable speed technology for temperature control in indirect evaporative cooling system. Applied Energy. 2019;251:113390.
[35] Price C, Rasmussen BP. Optimal tuning of cascaded control architectures for nonlinear HVAC systems. Science and Technology for the Built Environment. 2017;23:1190-202.
[36] Xiong Q, Cai W-J. Effective transfer function method for decentralized control system design of multi-input multi-output processes. Journal of Process Control. 2006;16:773-84.
[37] Luan X, Chen Q, Liu F. Equivalent transfer function based multi-loop PI control for high dimensional multivariable systems. International Journal of Control, Automation and Systems. 2015;13:346-52.
[38] Shen Y, Cai W-J, Li S. Normalized decoupling control for high-dimensional MIMO processes for application in room temperature control HVAC systems. Control Engineering Practice. 2010;18:652-64.
[39] He X-D. Dynamic modeling and multivariable control of vapor compression cycles in air conditioning systems Boston: Massachusetts Institute of Technology; 1997.
[40] Liang N, Shao S, Tian C, Yan Y. Dynamic simulation of variable capacity refrigeration systems under abnormal conditions. Applied Thermal Engineering. 2010;30:1205-14.
[41] Zhang W-J, Zhang C-L. A generalized moving-boundary model for transient simulation of dry-expansion evaporators under larger disturbances. International Journal of Refrigeration. 2006;29:1119-27.
[42] Rasmussen BP, Shenoy B. Dynamic modeling for vapor compression systems—Part II: Simulation tutorial. HVAC&R Research. 2012;18:956-73.
[43] Zhang CL. Fundamentals of Vapor-Compression Refrigeration and Air-Conditioning System Modeling. Beijing: Chemical Industry Press; 2012.
[44] GB/T-18837. Multi-split air conditioning (heat pump) unit. Peking (in Chinese): Standards Press of China; 2002.
[45] Lee Y, Park S, Lee M, Brosilow C. PID controller tuning for desired closed-loop responses for SI/SO systems. AIChE Journal. 1998;44:106-15.
[46] Camacho EF, Bordons C. Model predictive control. Advanced textbooks in control and signal processing. London: Springer-Verlag; 2004.